Reluctance Torque Evaluation for Interior Permanent Magnet Machines Using Frozen Permeability

X. Chen[*], J. Wang[*], V. I. Patel[*], P. Lazari[*], L. Chen[*] and P. Lombard[†]

[*]*Dept. of Electronic and Electrical Engineering, The University of Sheffield, Sheffield S1 3JD, UK*
xiao.chen@sheffield.ac.uk, j.b.wang@sheffield.ac.uk
[†]*CEDRAT S.A., 15 chemin de Malacher-Inovallée, 38246 MEYLAN Cedex, France*
patrick.lombard@cedrat.com

Keywords: Torque separation, reluctance torque, interior permanent magnet machine, frozen permeability.

Abstract

This paper proposes an accurate model which allows for separation of torque components based on frozen permeability concept for interior permanent magnet machines. An additional torque component due to the interaction of the rotor magnetic field with unequal *d* and *q*-axis reluctances in the stator iron is included. The proposed model can reproduce the instantaneous torque waveform at any load condition, and hence provides a more accurate means of reluctance torque evaluation compared with the conventional methods.

List of symbols

m	Number of phases
p	Number of pole pairs
ω	Rotational speed
θ	Rotor position angle
i_d	*d*-axis current
i_q	*q*-axis current
Ψ_d	*d*-axis flux linkage
Ψ_q	*q*-axis flux linkage
Ψ_{md}	*d*-axis PM flux linkage
Ψ_{mq}	*q*-axis PM flux linkage
L_d	*d*-axis self-inductance
L_q	*q*-axis self-inductance
M_{dq},M_{qd}	Mutual inductance between *d* and *q*-axis magnetic paths
T_{em}	Electromagnetic torque
T_{rel}	Reluctance torque

1 Introduction

The torque production of an interior permanent magnet (IPM) machine is contributed by both the alignment torque due to magnets and the reluctance torque due to rotor saliency. From the machine design point of view, a high reluctance torque ratio can increase torque production and overloading capability, enhance power density, and improve flux weakening performance of an IPM machine [1-3]. Therefore, an accurate evaluation of reluctance torque contribution is important to the IPM design.

The classic torque equation given in Equation (1) consists of two terms. The first term, known as alignment torque, is associated with the torque due to permanent magnet field, and the second term, known as reluctance torque, results from the difference in rotor *d* and *q*-axis reluctances.

$$T_{em} = \frac{m}{2} p \left\{ \Psi_m(i_d, i_q, \theta) i_q + \left[L_d(i_d, i_q, \theta) - L_q(i_d, i_q, \theta) \right] i_d i_q \right\} \quad (1)$$

In literature, a few methods have been presented to separate torque components, which include (a) modelling machine assuming constant PM flux linkage, (b) modelling machine assuming the PM flux linkage varies with *q*-axis current only [4] and (c) using frozen permeability (FP) concept [5-9]. The first two methods cannot separate PM flux linkage from the *d*-axis flux linkage correctly because the superposition principle is no longer valid in a non-linear system. In contrast, the FP concept is more preferable for torque separation. However, the torque separation is performed with the FP concept on average sense, not instantaneously in [9].

In this paper, an analytical model in transient FP process is presented, accounting for saturation effects in both *d* and *q*-axis magnetic circuits. Subsequently, the electromagnetic torque is separated into various components according to (a) classic torque equation, (b) classic torque equation derived from the FP concept and (c) the proposed torque equation also based on the FP approach. The torque calculated by these three different methods are then compared to show the improved torque prediction achieved by the proposed model.

2 Analytical model

Magnetic saturation in electrical machines can vary considerably with the electric loading of the machine. Under low load condition the magnetic saturation is low, and therefore the *d* and *q*-axis magnetic circuits are effectively independent and their mutual coupling is negligible. Hence, the *d* and *q*-axis flux linkages are expressed by Equation (2).

$$\begin{aligned} \Psi_d &= \Psi_m(i_d, i_q, \theta) + L_d(i_d, i_q, \theta) i_d \\ \Psi_q &= L_q(i_d, i_q, \theta) i_q \end{aligned} \quad (2)$$

However, when the torque demand is high, the shared magnetic paths of *d* and *q*-axes will be highly saturated and therefore the *d* and *q*-axis cross coupling effect has to be

taken into account for a high-fidelity machine model. It is arguable that the *d* and *q*-axis cross coupling effect may be represented in Equation (2) with variations of Ψ_m, L_d and L_q as functions of the *d* and *q*-axis currents. However, it implies that the *d*-axis current does not contribute to the *q*-axis flux linkage and vice versa. This relationship is not consistent with observations from finite element analysis (FEA) in that if a large positive *d*-axis current is injected while the *q*-axis current is kept zero, the resultant *q*-axis flux linkage may not be zero, due to magnetic coupling between the *d* and *q* axes at high saturation level. To account for the cross-coupling effect, mutual inductances are introduced to the *d* and *q*-axis flux linkages given in Equation (3).

$$\begin{aligned}\Psi_d &= \Psi_{md}(i_d, i_q, \theta) + L_d(i_d, i_q, \theta) i_d + M_{dq}(i_d, i_q, \theta) i_q \\ \Psi_q &= \Psi_{mq}(i_d, i_q, \theta) + M_{qd}(i_d, i_q, \theta) i_d + L_q(i_d, i_q, \theta) i_q\end{aligned} \quad (3)$$

The electromagnetic torque can be calculated by either Maxwell stress tensor method or virtual work principle. However, the Maxwell stress tensor method is sensitive to mesh density and quality as well as selection of the surface on which the Maxwell stress tensor is evaluated. Therefore, in this paper only the virtual work principle is employed in the torque calculation and all the FEA results are obtained via FLUX 2D software developed by CEDRAT [10].

The well-known equation for the torque production in the *dq* frame is shown in Equation (4). Substituting Equation (3) into Equation (4), the torque equation can be written as Equation (5).

$$T_{em} = \frac{m}{2} p \left[\Psi_d(i_d, i_q, \theta) i_q - \Psi_q(i_d, i_q, \theta) i_d \right] \quad (4)$$

$$T_{em} = \frac{m}{2} p \left[\Psi_{md} i_q - \Psi_{mq} i_d + \left(L_d - L_q\right) i_d i_q + M_{dq} i_q^{\,2} - M_{qd} i_d^{\,2} \right] \quad (5)$$

However, Equation (5) cannot be directly applied to the FP process, since it does not include the torque produced as a result of variation of magnetic co-energy [11]. To separate torque components accurately, a new torque equation in the FP process is proposed, as shown in Equation (6).

$$\begin{aligned}T_{em} = &\frac{m}{2} p \left[\Psi_{md} i_q - \Psi_{mq} i_d + \left(L_d - L_q\right) i_d i_q + M_{dq} i_q^{\,2} - M_{qd} i_d^{\,2} \right] \\ &+ T_{mr}\end{aligned} \quad (6)$$

where, T_{mr} represents the torque component contributed by the interaction of the rotor permanent magnet field with unequal reluctances in the *d* and *q*-axis directions in the stator iron. The physical interpretation of this torque component is understood by the fact that when permeability in an IPM machine is frozen for a given set of *d* and *q*-axis currents at a given rotor position, the reluctances in the *d* and *q*-axes in the stator will be different due to saturation effect, as shown in Fig. 1. Fig. 1 (a) and (b) illustrates the relative permeability contour of the rotor and stator laminations at 0° and 5° (half slot pitch) rotor positions with respect to phase *A* winding axis for a 10kW IPM machine with 36-slot 6-pole winding configuration. The selected working point is the rated torque

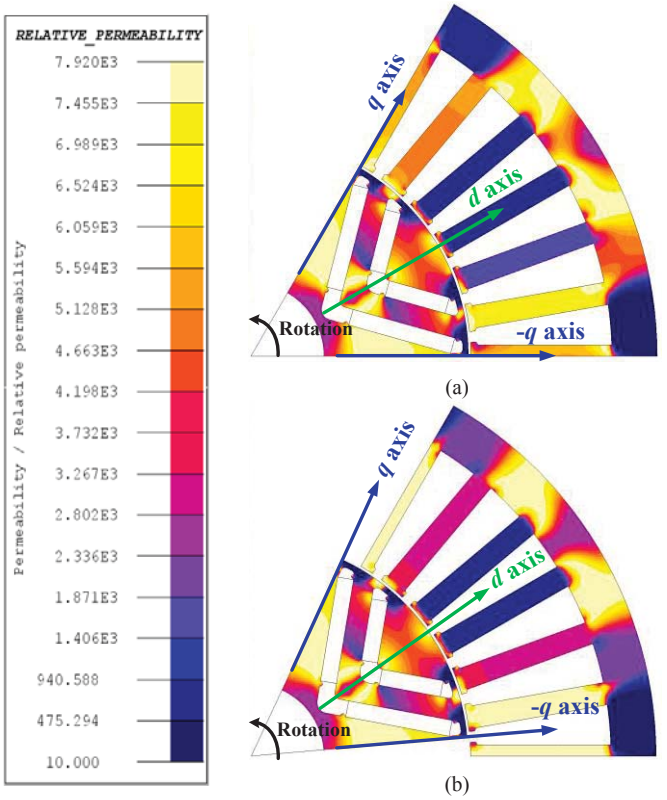

Fig. 1. Relative permeability contour at rated torque and base speed working point. (a) Rotor position θ=0°. (b) θ=5°.

Quantity	Unit	Value
Peak torque	Nm	70
Rated torque	Nm	35
Base Speed	rpm	1350
Max Speed	rpm	4500
Peak power	kW	9.9
Rated power	kW	5
DC link voltage	V	120
Peak current	A	125
Number of pole-pairs	--	3
Number of slots	--	36
Active stack length	mm	118
Stator outer diameter	mm	150
Rotor outer diameter	mm	80

Table 1. Specification and design parameters of machine prototype.

at the base speed and the machine specification and design details are listed in Table 1.

From Fig. 1 it can be seen that the permeability in the *d* and *q*-axes in the stator are different, and the average *q*-axis stator permeability is higher than that of the *d*-axis at both 0° and 5°. The unequal reluctances in the *d* and *q*-axis magnetic paths in the stator iron interact with the rotor permanent magnetic field, giving rise to the torque component T_{mr} in the same principle as a synchronous reluctance machine However, this torque component occurs even if the currents are zero.

3 Torque separation

To separate the instantaneous torque components in Equation (6), the specific FP process is needed, as described in the following sections.

3.1 FP concept

The basic FP concept is illustrated in Fig. 2, where the subscripts "*PM*", "*i*" and "*combined*" indicate PM excitation, current excitation and both PM and current excitation, respectively [9]. The combined magneto-motive (magnetic field strength) $H_{combined}$ is the sum of H_{PM} and H_i.

The working points on the B-H curve under the three excitations $H_{combined}$, H_{PM} and H_i are marked as "*a*", "*b*" and "*c*", respectively, and the resultant flux densities are denoted by $B_{combined}$, B_{PM} and B_i, respectively. It can be seen that $B_{PM}+B_i>B_{combined}$, indicating that the flux density of the combined field cannot be obtained by superimposing those from the PM and current excitations separately.

However, if the concept of FP is employed, the apparent relative permeability will be fixed at a specific value $\mu_{combined}$. In other words, the B-H relationship is no longer a non-linear B-H curve but a straight line with a slope of $\mu_{combined}$. Therefore, the working points under H_{PM} and H_i excitations are points "*d*" and "*e*", where the flux densities are B_{PM_FP} and B_{i_FP}. In this case, the $B_{combined}$ equals to the sum of B_{PM_FP} and B_{i_FP}. Hence the superposition principle can be used under FP condition.

3.2 FP process

In order to separate the torque components in Equation (6) using the concept of frozen permeability, a sequence of dedicated processes in one electrical period as illustrated in the flow chart of Fig. 3 has to be performed.

First, the magnetic fields in the machine at a given operating condition are solved by time-stepped FE over one electrical period. At each time step or each rotor position, relative permeability of each element in the stator and rotor cores are stored as spatial quantities. Thereafter, the magnetic properties for the stator and rotor cores are updated from the original B-H curves to the spatial quantities at the current time step. Subsequently, the excitation sources are changed according to the descriptions in the 2nd column in Table 2. By way of example, to calculate "*A*", FE analysis is performed by "Remove magnets" or setting the remanence of the magnets to zero while the current excitation is kept as required. After all the components in Table 2 are computed, the permeability of stator and rotor cores will be updated using the spatial quantities at the next time step. This process will continue until one electrical period is over.

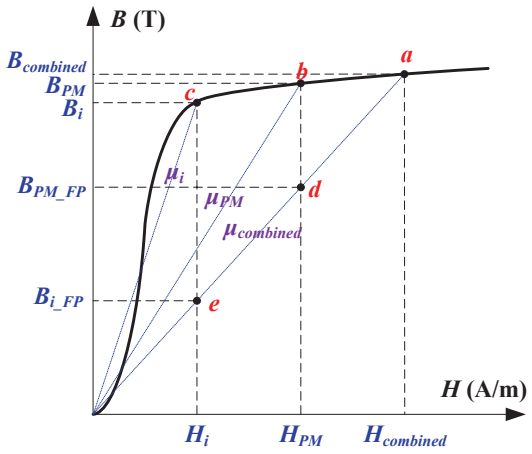

Fig. 2. FP concept diagram.

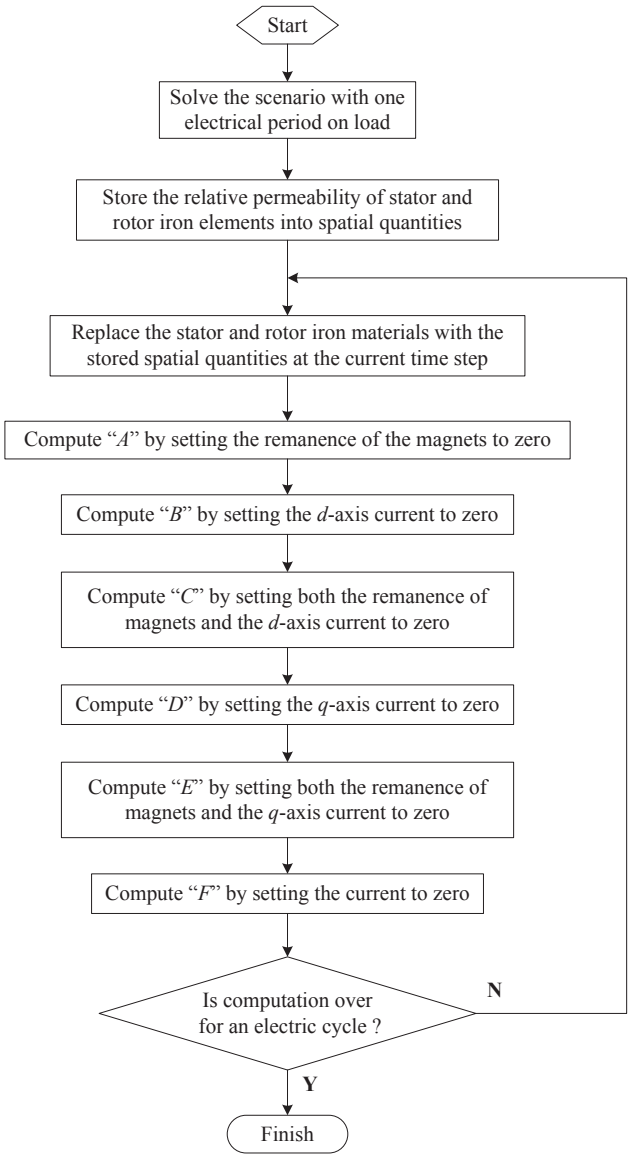

Fig. 3. Flow chart of transient FP process.

Torque terms	Description	Equation
A	Remove magnets	$\frac{m}{2}p\left[\left(L_d - L_q\right)i_d i_q + M_{dq}{i_q}^2 - M_{qd}{i_d}^2\right]$
B	No *d*-axis current	$\frac{m}{2}p\left[\Psi_{md} i_q + M_{dq}{i_q}^2\right] + T_{mr}$
C	Remove magnets & no *d*-axis current	$\frac{m}{2}pM_{dq}{i_q}^2$
D	No *q*-axis current	$\frac{m}{2}p\left[-\Psi_{mq} i_d - M_{qd}{i_d}^2\right] + T_{mr}$
E	Remove magnets & no *q*-axis current	$-\frac{m}{2}pM_{qd}{i_d}^2$
F	No current	T_{mr}

Table 2. Torque components separation in the FP process.

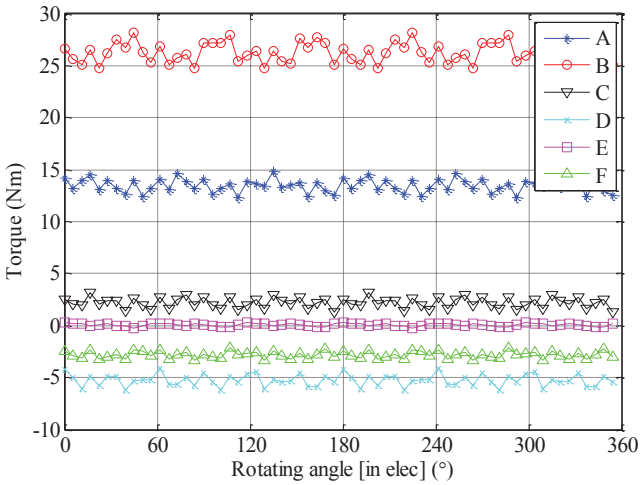

Fig. 4. Torque component waveforms at rated torque and base speed.

3.3 Torque components

Based on the FP process described in Fig. 3, the torque in Equation (6) can be separated into several components listed in Table 2 and rewritten as Equation (7):

$$T_{em} = A + B - C + D - E - F \tag{7}$$

The torque components as listed in Table 2, at the rated torque and the base speed working point, are plotted in Fig. 4 and the average values are tabulated in Table 3. It can be seen that the component "*B*" has the largest contribution because it contains the alignment torque given by $m/2 \cdot p\Psi_{md} i_q$. The component "*A*" also exhibits significant contribution because it contains reluctance torque terms. The components "*C*" and "*E*" resulting from the cross coupling effect of *d* and *q*-axis magnetic paths are relatively small. It should be noted that the component "*F*" resulting from the interaction of the rotor magnetic field with unequal *d* and *q*-axis reluctances in the stator iron is negative. As seen from the permeability contours in Fig. 1, the region from –*q*-axis to *d*-axis in the stator iron exhibits higher permeability than the region from *d*-axis to *q*-axis. This unequal reluctance in these two regions interacts with the magnetic field produced by the permanent magnets in the rotor, resulting in to a negative torque.

Torque components	Mean torque (Nm)	Mean torque ratio (%)
A	13.5	38.6%
B	26.3	75.1%
C	2.2	6.3%
D	-5.3	-15.1%
E	0.1	0.3%
F	-2.8	-8.0%
Total (*A*+*B*-*C*+*D*-*E*-*F*)	35	100.0%

Table 3. Mean values of torque components at rated torque and base speed.

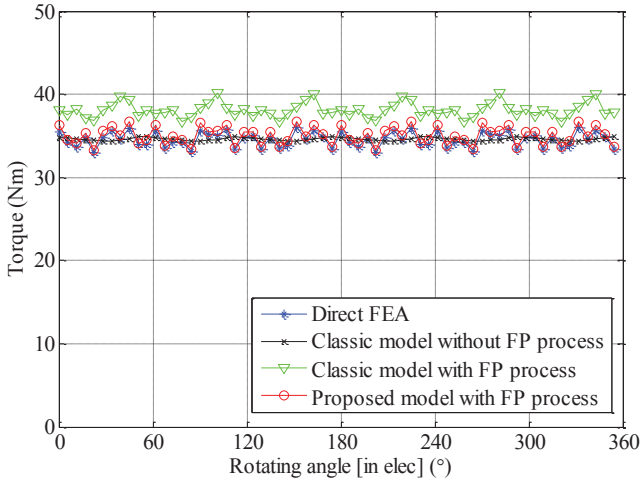

Fig. 5. Comparison of reproduced torque waveforms with direct FEA.

3.3 Torque reproduction

To validate the foregoing torque components separation, their sum according to Equation (7) is compared with that calculated directly by transient FEA in Fig. 5. It can be seen that the analytical model in Equation (6) based on the FP concept can accurately represent the torque production mechanism of the IPM machine.

In contrast, the classic torque equation in (8), which neglects the *d* and *q*-axis cross coupling effect and the term '*F*' in Table 2, can be obtained by the torque components listed in Table 2. However, the use of this equation with the FP concept results in a relatively large error when compared with the torque obtained by direct FEA or Equation (6), as shown in Fig. 5. This is due to the fact that the classic torque equation in (8) neglects the contribution of the *d* and *q*-axis mutual inductance to the reluctance torque and the influence of the unequal reluctances of the *d* and *q*-axis magnetic circuit in the stator iron on the alignment torque.

$$T_{em} = \frac{m}{2}p\left[\Psi_{md} i_q + \left(L_d - L_q\right)i_d i_q\right] = A + B - 2C - E - F \tag{8}$$

The alignment torque and reluctance torque in Equation (8) can also be separated by assuming that the *d*-axis flux linkage due to permanent magnets only varies with *q*-axis current, viz. the classic model without FP in Fig. 5. However, the total torque obtained with this assumption only matches the average torque of the direct FEA. A large deviation in the

instantaneous torques waveforms between the two exists, as shown in Fig. 5. This is because the torque components due to the cross coupling effect and the non-uniform reluctance in the stator core are not accounted in the classical model without FP. The high frequency ripples in the both components are therefore not present in the torque waveform obtained from the classical model.

Therefore, only the proposed Equation (6) can accurately represent the torque production mechanism of the IPM machine using the FP concept.

4 Reluctance torque evaluation

In this section, the reluctance torque calculation based on the classic torque equations and the proposed model is carried out and compared.

The reluctance torque according to the classic torque equation is given in Equation (9). This torque component may be obtained by assuming that the *d*-axis flux linkage due to permanent magnets is independent of *d*-axis current, or by computing terms "*A*", "*C*" and "*E*" as shown in Equation (9) with FP process. The reluctance torque based on the proposed equation can be evaluated according to Equation (10), or by computing term "*A*" with FP process. The reluctance torque comparison is shown in Fig. 6 and Table 4.

$$T_{rel} = \frac{m}{2} p\left[\left(L_d - L_q\right) i_d i_q\right] = A - C - E \qquad (9)$$

$$T_{rel} = \frac{m}{2} p\left[\left(L_d - L_q\right) i_d i_q + M_{dq} {i_q}^2 - M_{qd} {i_d}^2\right] = A \qquad (10)$$

It can be seen that the reluctance torque calculations based on the classic models with and without the FP process underestimate the reluctance torque compared with the proposed model with the FP process. This is attributable to two reasons. First, the classic models neglect the torque component contributed by the mutual inductance, viz. component "*C*" and "*E*" whose mean values are positive, which can be observed in Fig. 4 and Table 3. Secondly, the negative torque component T_{mr} shown in Fig. 4 resulting from the FP process is attributed to the alignment torque rather than the reluctance torque in both the classic model and proposed model with the FP process. This component is not present in the classical model without FP given by Equation (1). Consequently, the alignment torque predicted by the FP process is lower while the reluctance torque is higher compared with those predicted using the classical model without FP.

Separation of the two torque components with non-linear machine characteristics has to be based on an assumption, and the FP process is no exception. However, the torque separation based on the proposed FP concept should be more accurate than the classic approach that neglects the torque due to mutual coupling and assumes the PM flux linkage is independent with the *d*-axis current, both of which deviate more from the real physical condition at a high level of saturation.

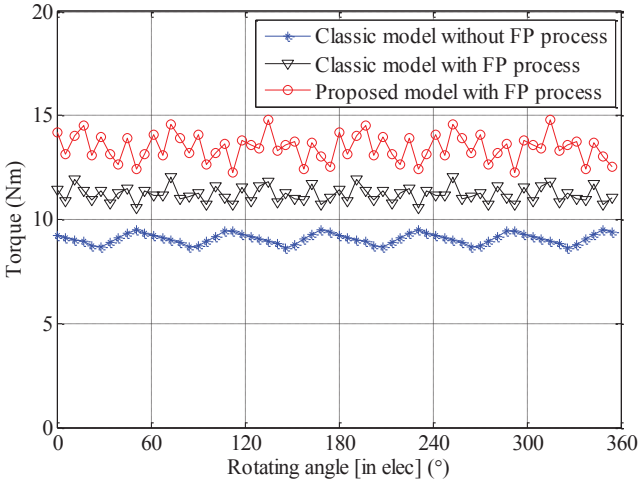

Fig. 6. Reluctance torque waveform comparison.

	Classic model without FP process	Classic model with FP process	Proposed model with FP process
Mean reluctance torque (Nm)	9.1	11.2	13.5
Mean reluctance torque ratio (%)	25.9%	32.0%	38.5%

Table 4. Reluctance torque comparison.

5 Conclusion

The paper shows that using the classic models, which assume that the PM flux linkage is independent with *d*-axis current, can only match the average total torque but not the instantaneous torque waveform. However, the proposed model can match both average and instantaneous torque very well with the direct FEA results.

A more accurate model which allows for separation of torque components via FP process for IPM machines is presented. The proposed model can reproduce the instantaneous torque waveform at any load condition, and hence provides a more accurate evaluation of reluctance torque compared with the conventional methods.

Acknowledgements

The authors would like to thank the European Commission for finance support under Grant No. 266084 and HIWI project partners for permission of publication of this paper. They also would like to thank Bhaskar Sen for valuable suggestions and discussions.

References

[1] L. Jung-Ho, Y.-J. Jang, and H. Jung-Pyo, "Characteristic analysis of permanent magnet-assisted synchronous reluctance motor for high power application," *Journal of Applied Physics,* vol. 97, pp. 10Q503-10Q503-3, (2005).

[2] S. Ooi, S. Morimoto, M. Sanada, and Y. Inoue, "Performance evaluation of a high-power-density pmasynrm with ferrite magnets," *Industry Applications, IEEE Transactions on,* vol. 49, pp. 1308-1315, (2013).

[3] H. Murakami*, et al.*, "Optimum design of highly efficient magnet assisted reluctance motor," in *Industry Applications Conference, 2001. Thirty-Sixth IAS Annual Meeting. Conference Record of the 2001 IEEE*, 2001, pp. 2296-2301 vol.4.

[4] G. Qi*, et al.*, "Influence of skew and cross-coupling on flux-weakening performance of permanent-magnet brushless ac machines," *Magnetics, IEEE Transactions on,* vol. 45, pp. 2110-2117, (2009).

[5] N. Bianchi and S. Bolognani, "Magnetic models of saturated interior permanent magnet motors based on finite element analysis," in *Industry Applications Conference, 1998. Thirty-Third IAS Annual Meeting. The 1998 IEEE*, 1998, pp. 27-34 vol.1.

[6] J. K. Tangudu, T. M. Jahns, A. M. El-Refaie, and Z. Q. Zhu, "Segregation of torque components in fractional-slot concentrated-winding interior pm machines using frozen permeability," in *Energy Conversion Congress and Exposition, 2009. ECCE 2009. IEEE*, 2009, pp. 3814-3821.

[7] J. A. Walker, D. G. Dorrell, and C. Cossar, "Flux-linkage calculation in permanent-magnet motors using the frozen permeabilities method," *Magnetics, IEEE Transactions on,* vol. 41, pp. 3946-3948, (2005).

[8] K. Sang-Yeop, K. Jae-Kwang, and J. Hyun-Kyo, "Characteristic analysis of multilayer-buried magnet synchronous motor using fixed permeability method," *Energy Conversion, IEEE Transactions on,* vol. 20, pp. 549-555, (2005).

[9] W. Q. Chu and Z. Q. Zhu, "Average torque separation in permanent magnet synchronous machines using frozen permeability," *Magnetics, IEEE Transactions on,* vol. 49, pp. 1202-1210, (2013).

[10] CEDRAT. (2013). *Flux v11.1.2 user manual*. Available: http://www.cedrat.com/en/software/flux.html

[11] N. Bianchi and L. Alberti, "Mmf harmonics effect on the embedded fe analytical computation of pm motors," *Industry Applications, IEEE Transactions on,* vol. 46, pp. 812-820, (2010).